Ultralightweight and 3D Squeezable Graphene-Polydimethylsiloxane Composite Foams as Piezoresistive Sensors

Sengupta, Debarun; Pei, Yutao; Kottapalli, Ajay Giri Prakash

Published in:
ACS Applied Materials & Interfaces

DOI:
10.1021/acsami.9b11776

Publication date:
2019

ACS APPLIED MATERIALS & INTERFACES

Research Article

Cite This: ACS Appl. Mater. Interfaces 2019, 11, 35201−35211

www.acsami.org

Ultralightweight and 3D Squeezable Graphene-Polydimethylsiloxane Composite Foams as Piezoresistive Sensors

Debarun Sengupta,[†] Yutao Pei,[†] and Ajay Giri Prakash Kottapalli*[,†,‡]

[†]Department of Advanced Production Engineering (APE), Engineering and Technology Institute Groningen (ENTEG), University of Groningen, Groningen 9747 AG, The Netherlands

[‡]MIT Sea Grant College Program, Massachusetts Institute of Technology (MIT), 77 Massachusetts Avenue, NW98-151, Cambridge, Massachusetts 02139, United States

Supporting Information

ABSTRACT: The growing demand for flexible, ultrasensitive, squeezable, skin-mountable, and wearable sensors tailored to the requirements of personalized health-care monitoring has fueled the necessity to explore novel nanomaterial-polymer composite-based sensors. Herein, we report a sensitive, 3D squeezable graphene-polydimethylsiloxane (PDMS) foam-based piezoresistive sensor realized by infusing multilayered graphene nanoparticles into a sugar-scaffolded porous PDMS foam structure. Static and dynamic compressive strain testing of the resulting piezoresistive foam sensors revealed two linear response regions with an average gauge factor of 2.87−8.77 over a strain range of 0−50%. Furthermore, the dynamic stimulus−response revealed the ability of the sensors to effectively track dynamic pressure up to a frequency of 70 Hz. In addition, the sensors displayed a high stability over 36000 cycles of cyclic compressive loading and 100 cycles of complete human gait motion. The 3D sensing foams were applied to experimentally demonstrate accurate human gait monitoring through both simulated gait models and real-time gait characterization experiments. The real-time gait experiments conducted demonstrate that the information of the pressure profile obtained at three locations in the shoe sole could not only differentiate between different kinds of human gaits including walking and running but also identify possible fall conditions. This work also demonstrates the capability of the sensors to differentiate between foot anatomies, such as a flat foot (low central arch) and a medium arch foot, which is biomechanically more efficient. Furthermore, the sensors were able to sense various basic joint movement responses demonstrating their suitability for personalized health-care applications.

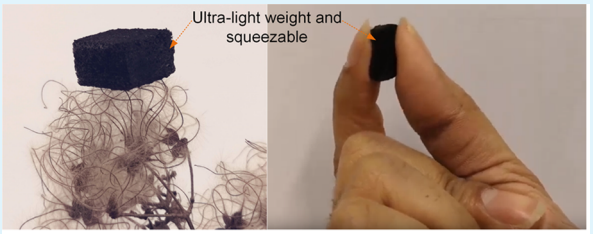

Ultra-light weight and squeezable graphene-PDMS foam for piezoresistive sensing

KEYWORDS: *multilayer graphene, piezoresistive sensor, squeezable sensor, flexible sensor, gait monitoring*

1. INTRODUCTION

The growing demand for flexible, ultrasensitive wearable sensors for myoelectric prosthesis, soft robotics, and personalized health monitoring applications has been the main driving factor behind the rapid advancement in soft and flexible material processing technologies. In particular, human motion monitoring devices are emerging to be the most sought-after wearable devices as they can potentially provide a host of valuable information regarding the health and well-being of an individual. For example, gait monitoring in individuals suffering from Parkinson's disease, stroke, multiple sclerosis, and other neurological conditions can provide valuable information regarding the progression of the diseases, and hence, continuous monitoring of gait characteristics can enable early diagnosis, subsequently enabling personalized treatment plans for patients.[1] Accurate monitoring of human gait and other human motion parameters like joint and limb movements necessitates the availability of squeezable, skin-mountable, low-cost, and durable sensors.

Traditionally, piezoelectric, piezoresistive, and capacitive transduction mechanisms have mostly been exploited in the development of flexible sensors to convert strain stimuli into electrical signals. Inorganic piezoelectric materials such as lead zirconate titanate, zinc oxide (ZnO), barium titanate ($BaTiO_3$),[2−7] and soft piezoelectric polymers like polyvinylidene fluoride (PVDF) and polyvinylidene fluoride-trifluoroethylene (PVDF-TrFE)[8−12] have been explored extensively for developing various flexible sensors in the past. On the other hand, though piezoresistive microelectromechanical system sensors using metallic- and semiconductor-based strain gauges have been quite popular for strain sensing applications owing to their well-established fabrication processes and large measurement range, their application as wearable sensors is limited due to their high stiffness and low stretchability.[13,14] Flexible and squeezable sensors utilizing the piezoresistive property of nanomaterial-elastomer composites are relatively new, and researchers across the globe have been exploring various combinations of novel nanomaterials and suitable

Received: July 5, 2019
Accepted: August 28, 2019
Published: August 28, 2019

DOI: 10.1021/acsami.9b11776
ACS Appl. Mater. Interfaces 2019, 11, 35201−35211

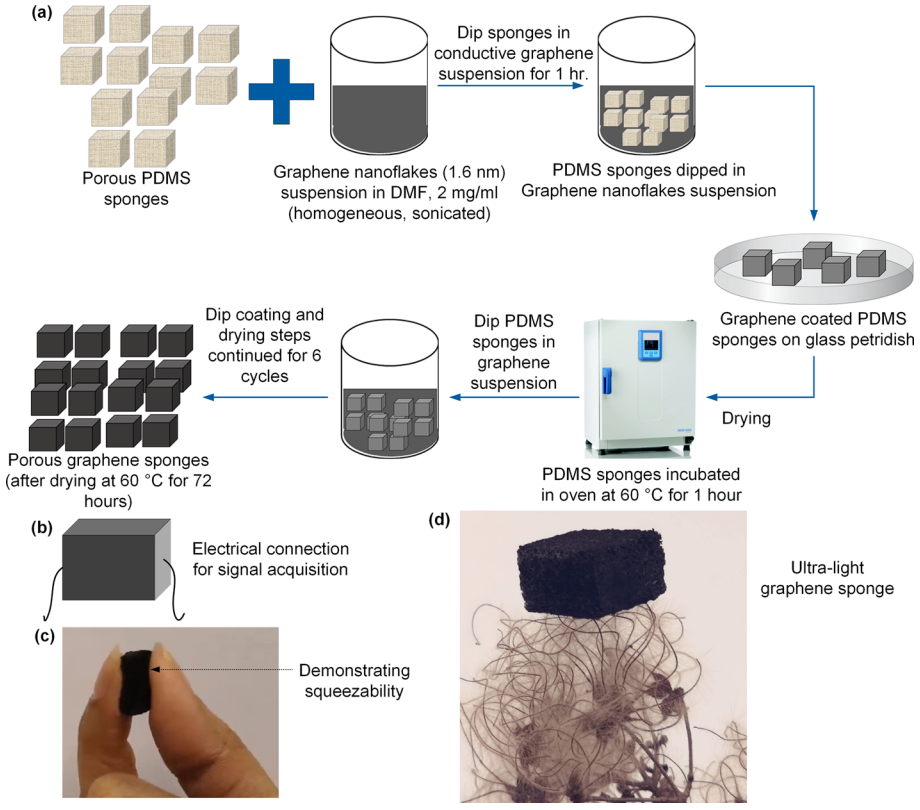

Figure 1. Fabrication of the squeezable graphene-PDMS foam sensor: (a) schematic representation of infiltrating PDMS foam with multilayered graphene nanoflakes (MLG); (b) schematic representation of a single PDMS-MLG foam sensor with electrical contacts; (c) squeezability and (d) ultralight nature of the graphene-PDMS foam sensor.

elastomers for developing a new generation of innovative, flexible piezoresistive sensors.[15−21] Polymer materials like polydimethylsiloxane (PDMS), ecoflex, polyimide (PI), rubber, and polyurethane (PU) have been commonly used as flexible polymer substrates due to their superior flexibility compressibility and excellent responsiveness to torsion, tension, and compression.[16,18,22−24] To make the sensors low cost, renewable, and biodegradable, a recent work reported the use of a printing paper substrate as a novel alternative to traditional elastomers.[25] For the conductive nanomaterials, silver nanowires (AgNWs) and various types of carbon-based materials like carbon nanotubes (CNTs), carbon nanofibers (CNFs), carbon blacks, and graphene have been explored by researchers.[18,19,26−32] Of all the conductive carbon-based nanomaterials, recently, graphene has been exploited the most for developing nanomaterial-polymer composite-based piezoresistive sensors mainly because of its excellent conductivity, stiffness, and elastic properties.[16,22,33] The most common method of developing graphene-based piezoresistive sensors has been the use of nanoporous graphene foams synthesized by chemical vapor deposition. Due to the fragility of freestanding 3D graphene foams, they are infiltrated with elastomers like PDMS to enhance their mechanical properties like elasticity and durability. Pang et al. proposed a novel method involving infiltration of PDMS in a graphene-coated nickel foam template and subsequent etching to preserve the graphene nanoporous structure with the PDMS scaffold for developing a highly sensitive piezoresistive sensor.[16] Recently, researchers have also reported graphene-based fiber sensors for various strain monitoring applications.[31,34] A recently published review article presents a detailed overview of the developments in the field of flexible polymer-based strain sensors and discusses the recent developments in the field of electrically conductive polymer composites.[35]

Most of the graphene-elastomer foam/spongy materials reported so far have either employed fragile freestanding foamy graphene structures or involved sophisticated multistep fabrication methods involving polymer infiltration in a graphene-coated template and subsequent etching. In addition, most of these works focused on the synthesis of the spongy nanomaterials; however, their applications as sensing materials to develop 3D squeezable sensors were not investigated.[36−38] In this work, we propose a facile process of developing an ultralightweight and highly squeezable 3D microporous graphene-PDMS foam-based sensor. Sugar cubes were used as templates for developing microporous PDMS foams followed by dip coating of the foams in conductive multilayered graphene (MLG) suspension to infiltrate them with graphene nanoflakes. The porous graphene-infiltrated foams were studied employing a scanning electron microscope (SEM) to understand its strain-induced resistance modulation mechanism, and the conductive domain disconnection mechanism was invoked to explain its piezoresistive property. The density of the graphene-PDMS foam sensors was calculated to be 0.305 g cm^{-3} owing to the porous structure. The response of the graphene-PDMS sensors developed with the proposed method was characterized for static and dynamic pressure stimuli. From the static and dynamic compressive strain tests, the response of the sensor was found to have two linear regions with an average gauge factor lying in the range of 2.87−8.77. Accelerated lifetime tests were conducted on the spongy sensor through cyclic compressive loading involving

DOI: 10.1021/acsami.9b11776
ACS Appl. Mater. Interfaces 2019, 11, 35201−35211

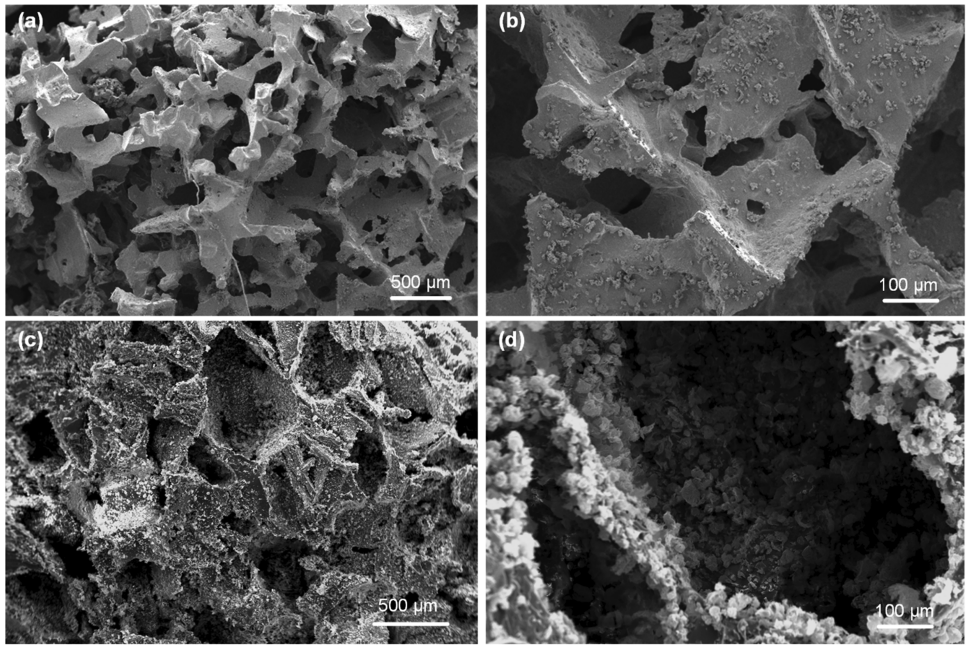

Figure 2. SEM micrographs of the PDMS foam before and after MLG loading: (a,b) porous structure of the unloaded PDMS foam at different magnifications; (c,d) MLG-loaded PDMS foam at two different magnifications with the pore walls covered with MLG nanoflakes forming a nanomaterial percolation network.

36000 load cycles to demonstrate its overall reliability and durability. The responses of the sensors to dynamic loading were characterized to observe their sensing performances at high-frequency strain loading. Finally, the application of these sensors in monitoring both simulated and real-time human gaits and other body motion parameters was validated through experiments that demonstrate the broad applicability of such sensors in various applications including personalized health monitoring, soft robotics, myoelectric prosthesis, and other wearable devices. Three identical sensors were assembled on a soft shoe sole and used in synchronization to differentiate between the pressure profiles under a low arch/flat foot and a medium arch foot. The sensor assembly was also used for demonstrating the capability for real-time gait characteristic acquisition and differentiation between different kinds of human movements, including walking, running, periodic leaning, and standing. The simple method of sensor development demonstrated in this work will guide the development of a future generation of 3D squeezable and highly sensitive pressure/strain sensors suitable for various high-performance, wearable, and flexible devices.

2. RESULTS AND DISCUSSION

2.1. 3D Squeezable Graphene-PDMS Foam Sensor. *2.1.1. Sensor Fabrication and Morphological Study.* The process steps involved in fabrication of the graphene-PDMS squeezable strain sensor are schematically illustrated in Figure 1a. The experimental details of the fabrication process are described in the Experimental Methods section. The electrical connections for acquiring electrical outputs from the sensor were made by smearing and subsequently curing a thin layer of conductive silver epoxy on the two sides of the graphene-PDMS foam as shown in Figure 1b. The optical images shown in Figure 1c,d demonstrate the compressibility and ultralightweight of the developed sensor, respectively. Furthermore, the squeezability of the sensor was demonstrated by holding it between two fingers and applying a series of squeeze−release cycles (shown in Video S1).

Multiple dip coating and drying cycles of the PDMS sponge in homogeneous graphene/*N*,*N*-dimethylformamide (DMF) suspension led to the attachment of multilayered graphene nanoflakes (MLG) in the inner pore walls of the microporous PDMS substrate. Figure 2a,b shows the SEM micrographs of the unloaded PDMS foam. An average pore diameter of 386 μm was observed for the developed PDMS foam (averaged over eight measurements on different sponges). Figure 2c,d shows the SEM micrographs after loading the PDMS with MLG. As the SEM micrographs clearly depict, the graphene nanoflakes penetrated into the porous structure of the PDMS foam and attached themselves onto the inner walls of the microporous structure.

The strain-responsive resistance change mechanism in the graphene-PDMS foam could arise from the conductive domain disconnection mechanism, which was also reported in the past for other types of thin films made of nanomaterials.[19,24,39−41] Within the MLG nanomaterial flake network, electrons pass through the overlapping network of conductive MLG flakes. Application of external force/stress causes a change in the overlapping area between the conductive MLG flakes, thus leading to a change in resistance as schematically explained in Figure 3a. Also, electrons can tunnel across a thin polymer barrier separating two adjacent nanomaterial domains, thus forming quantum tunneling junctions. The tunneling resistance between two adjacent graphene nanoflakes separated by a polymer layer can be predicted using Simmon's tunneling resistance theory.[42] In the past, researchers have reported a tunneling cutoff distance of 2−3 nm between two parallel graphene sheets separated by polymer insulation.[43,44] Upon application of pressure, a pore wall may get compressed enough so that the effective distance between two graphene nanoflakes adhering to the opposite sides of the wall may reduce to 2 nm or less in which case electrons will be able to

DOI: 10.1021/acsami.9b11776
ACS Appl. Mater. Interfaces 2019, 11, 35201−35211

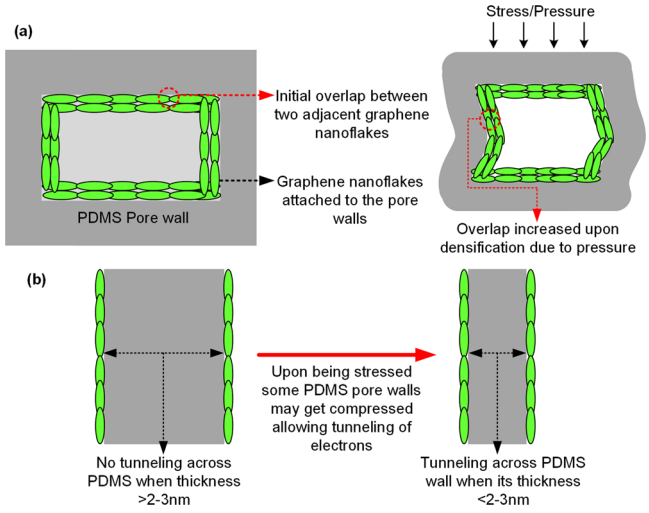

Figure 3. Schematic diagram explaining the possible strain-induced resistance modulation mechanisms in graphene-PDMS foam sensor: (a) schematic explaining the conductive domain disconnection mechanism explaining strain-induced resistance modulation observed in the sensor; (b) schematic representation of stress-induced tunneling resistance modulation.

tunnel across the PDMS wall barrier. Figure 3b schematically explains the stress-induced tunneling resistance modulation. Given the relatively large size of the pores, it can be safely assumed that the strain-responsive piezoresistivity in the graphene-PDMS foams reported in this paper originates mostly due to the conductive domain disconnection mechanism (while the stress-induced tunneling resistance modulation mechanism plays a minimal to no role at all) wherein an external force/stress causes the graphene nanoflakes to slide against each other, thus leading to a large change in overall resistance of the graphene-PDMS foam sensor.

2.1.2. Strain Sensor Characterization. The graphene-PDMS foam sensors were characterized under various strain loading conditions including static and dynamic loading in order to demonstrate its applications for flexible and wearable sensors. Figure 4a shows the schematic representation of the experimental setup used for the characterization of the sensors (details provided in the Experimental Methods section). An initial precompression of 1% was applied to avoid problems related to initial sliding/settling of graphene nanoflakes, which are observed in similar types of squeezable sensors developed in the past.[33] A compressive strain was applied in steps of 0.5% all the way up to 9.5%. After attaining a peak compressive strain of 9.5%, the strain was released in steps of 0.5% to return to the starting position. The experiment was repeated three times, and no noticeable delay was observed between the piston extension and the sensor response throughout the duration of the experiment. With increasing compressive strain, the resistance of the sensor was observed to decrease linearly for strains up to 9.5%. Figure 4b shows the plot of the modulus of normalized resistance change calculated from the data acquired from the Wheatstone bridge circuit versus the compressive strain. The output of the sensor was observed to increase linearly with increasing strain for compressive strains up to 9.5%. The data was treated with a linear regression fit to estimate the compressive gauge factor ($\mathrm{GF} = \frac{\Delta R}{R} / \frac{\Delta L}{L}$) of the graphene-PDMS foam. The compressive gauge factor of the sensor was determined to be 8.77 from the slope of the linear regression. To assess the strain sensing performance of the graphene-PDMS foam sensor for larger strains, the sensor was subjected to five different maximum compressive cyclic strains (10, 20, 30, 40, and 50%) at a constant frequency of 5 Hz using a minishaker setup as depicted in the schematic in Figure 4c (details of the experimental setup are provided in the Experimental Methods section). The minishaker was driven with a square-wave stimulus at a constant frequency of 5 Hz, which resulted in cyclic compressive stains in the sponge. The sensor outputs were recorded for at least 50 cycles at each of the aforementioned maximum strain levels, and the normalized resistance changes were calculated and plotted for the individual compressive strain cycles as shown in Figure 4d. Figure 4e shows the superimposed plots of the normalized resistance change demonstrated by the sensor in response to the five maximum compressive strain cycles (appropriate band-pass filter was used to eliminate the 50 Hz power supply interference). The data from the cyclic compressive strain characterization experiment were analyzed, and the mean normalized resistance change values were determined individually for each of the five different maximum compressive strain levels. Furthermore, the gauge factor of the sponge was determined individually for each of the aforementioned compressive strain values and plotted in the form of a bar graph, as shown in Figure 4f. From the plots in Figure 4b,f, two distinct regions of operations (of the graphene-PDMS foam sensor) can be identified. The sensor demonstrated a reasonably linear response for strain levels up to 9.5%. A sharp decrease in the gauge factor was observed for strains exceeding 10%. The decrease in the gauge factor at higher strain rates can be attributed to the fact that, at higher strain values, the internanoparticle distances are continuously bridged, and hence, the sensor reaches near network saturation.[45] Thus, saturation in the percentage decrease in resistance for higher compressive strain levels is observed, which is clearly reflected by the reduced gauge factor values (at higher strain levels exceeding 10%). Similar response characteristics have been observed for similar nanoparticle-elastomer composite foam-based sensors in the past.[16,45] Table 1 compares the gauge factor of our graphene-PDMS foam sensor with some other sensors reported by various researchers in the past.

2.1.3. Reliability Test and Dynamic Response Characterization. To demonstrate the long-time reliability of the graphene-PDMS foam sensor, an accelerated lifetime testing was conducted on the sensor by subjecting it to a series of 36000 cyclic compressive loading and unloading at 5% compressive strain using the same experimental setup previously shown in Figure4c. The minishaker was driven at a constant frequency of 10 Hz, and the power amplifier driving the setup was set such that the compressive strain generated was approximately 5%. The sensor response was acquired from the Wheatstone bridge circuit, and an appropriate band-pass filter was applied to eliminate the 50 Hz power supply interference. Figure 5a shows the normalized resistance change plots acquired from the reliability tests. A zoomed-in plot placed on the right-hand side of the main plot shows the consistency of the sensor response cycles for the applied cyclic compressive strains.

To further evaluate the strain sensing performance of the sensor under dynamic loading conditions, the graphene-PDMS foam sensor was subjected to compressive strains at three

DOI: 10.1021/acsami.9b11776
ACS Appl. Mater. Interfaces 2019, 11, 35201−35211

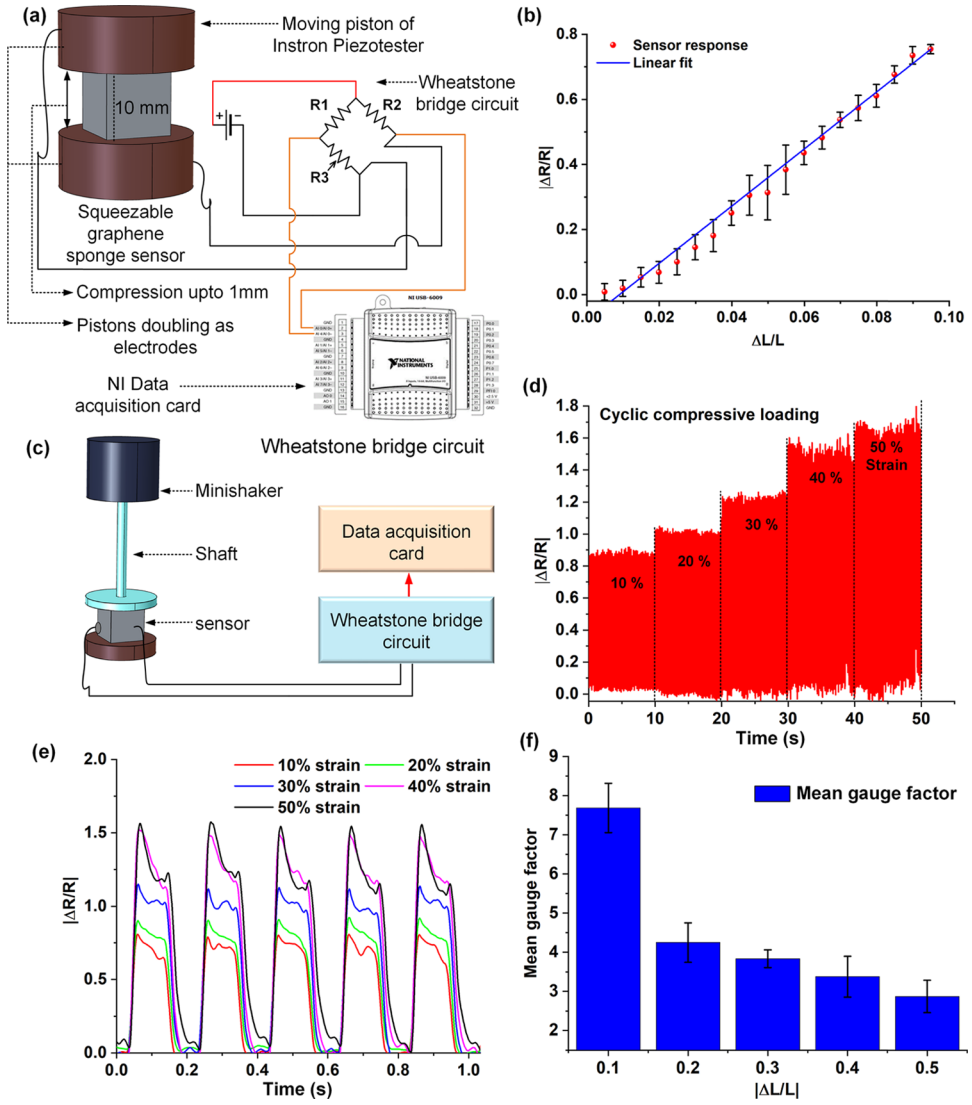

Figure 4. Graphene-PDMS foam sensor characterization: (a) schematic representation of the setup used for conducting the piezoresistivity characterization experiments; (b) plot of normalized resistance change in the graphene-PDMS foam sensor versus applied compressive strain up to 9.5%; (c) schematic representation of the setup used for conducting the piezoresistivity characterization experiments for larger compressive strains in the range of about 10−50%; (d) plot showing the sensor response in terms of normalized resistance change when subjected to five different compressive loading at different strains (between 10 and 50%); (e) superimposition plot showing the normalized resistance change of the sensor for five different compressive strains between 10 and 50%; (f) bar chart showing the calculated gauge factor for the graphene-PDMS foam sensor for the five different compressive strains between 10 and 50%.

Table 1. Summarizing the Gauge Factors of Various Flexible Strain Sensors Reported in the Past

material	gauge factor	linearity
AgNWs-PDMS[19]	2−14	linear up to 40%
CNTs-Ecoflex[18]	1−2.5	linear
aligned SWCNTs-PDMS[26]	0.82	two linear regions
carbon black-PDMS[27]	1.8−5.5	two linear regions
carbon black-EcoFlex[46]	3.8	nonlinear
single CNF strain sensor[47]	1.96−2.55	linear
GPN-PDMS[16]	2.6−8.5	two linear regions
graphene-rubber[24]	35	linear and exponential regions
graphene ink-on-PDMS[48]	37	linear
graphene-PDMS foam (this work)	2.87−8.77	two linear regions

different frequencies using the same minishaker setup described previously. The minishaker was driven with square-wave stimuli at three different frequencies (10, 35, and 70 Hz), which caused compression of the sponge at those frequencies. Figure 5b shows the as-acquired sensor response for the oscillatory test conducted at 10 Hz. For the 35 and 70 Hz stimuli, the sensor responses were acquired and treated with appropriate low-pass filters in order to eliminate the 50 Hz power supply interference. Fast Fourier transform (FFT) was carried out on the individual responses to determine the average amplitude of the sensor response as shown in Figure 5c. The sensor amplitude responses were observed to have increased with the applied stimulus frequency.

2.2. Sensor Applications. *2.2.1. Application of the Graphene-PDMS Foam for Human Motion Monitoring.* Continuous monitoring of gait characteristics can enable early diagnosis of diseases like stroke, multiple sclerosis, and

DOI: 10.1021/acsami.9b11776
ACS Appl. Mater. Interfaces 2019, 11, 35201−35211

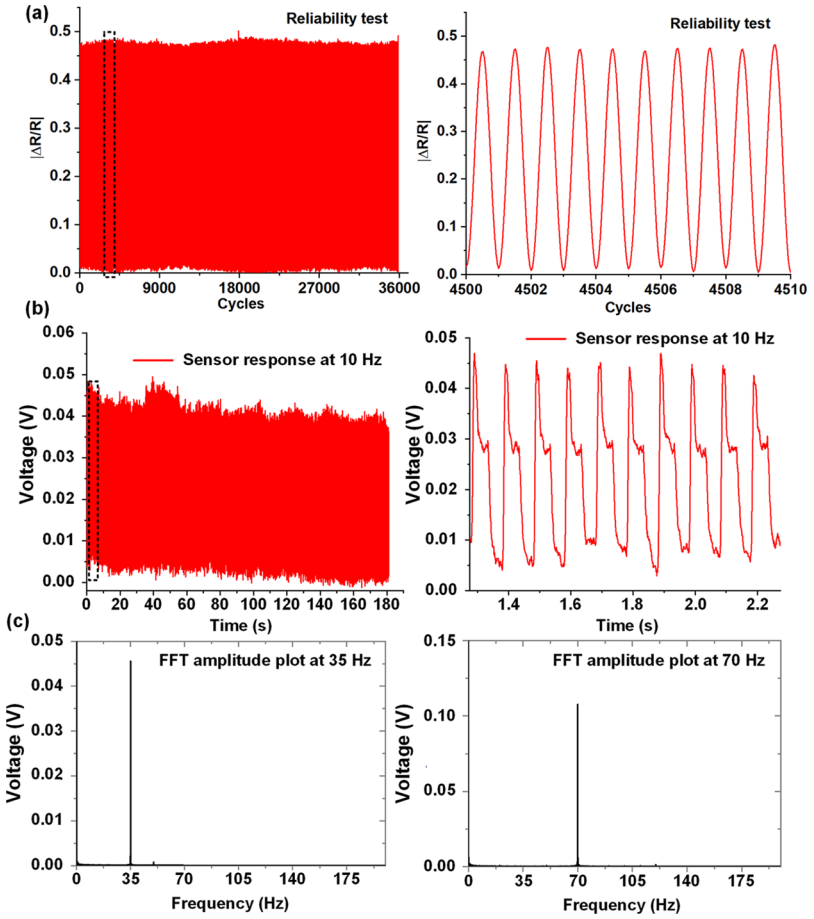

Figure 5. Cyclic compressive loading and dynamic strain sensing characterization of the graphene-PDMS foam sensor: (a) response of the sensor to cyclic loading and unloading at 5% compressive strain. The figure on the right shows the zoomed-in version of the plot; (b) plot showing the sensor response at 10 Hz in time domain; zoomed in plot on the right showing the sensor response at 10 Hz in the interval of 1.3−2.3 s; (c) FFT amplitude plots showing the sensor responses at 35 and 70 Hz.

Parkinson's disease, thus enabling personalized treatment plans for patients.[1] To demonstrate the applicability of the graphene-PDMS foam sensors in gait monitoring, a gait simulation response experiment was conducted using the Instron 5940 UTS (details of the experimental setup are provided in the Experimental Methods section). The pressure behavior under the heel of a walking person was appropriately mimicked employing simulated gait models applied to the movable piston of the test system. The pressure pattern under the heel of a walking individual comprises a gradual ramping up to the maximum pressure (body weight divided by the area of the heel pad) followed by a partial pressure release and finally ramping down to a complete pressure release when the heel is lifted off the ground.[49] Due to limitations of the test setup used, the force ramp up and ramp down rate was slow (20 mm/min movement of piston) due to which each gait cycle lasted 30 s unlike in real human being where each gait cycle lasts 1.08 ± 0.11 s.[50] The experiment was carried out for 45 gait cycle repetitions to demonstrate the consistency in sensor response. Figure 6a shows the sensor response for the gait simulation experiment. The zoomed-in version of Figure 6a (right) shows the sensor response for four complete gait cycles. The schematic diagrams in the figure inset explain the sensor response by comparing it to the heel movement. Overall, a good consistency was observed in the sensor response throughout the gait simulation experiment.

To demonstrate the capability of the sensor for real-time gait and foot pressure monitoring, three identical graphene-PDMS sensors were attached and secured on a soft flat shoe sole with the intention of acquiring the sensor response from three distinct pressure points (toe ball, foot arch, and heel) of the right foot as shown in Figure 6b. The shoe sole-sensor assembly (SSA) was placed inside a shoe and worn by a person with a medium arch foot. Figure 6c shows the response of the sensor (acquired in real time) while the person was walking slowly. For this work, the sensor responses from the toe ball and the heel regions are shown as these are the two most intense pressure regions in the medium arch biomechanically efficient foot. The phase lag between sensors from the toe ball and heel region demonstrates the walking behavior of the person. While walking, when the heel is placed down, the pressure increases to a maximum value followed by subsequent relaxation while the whole foot is placed down on the floor. At the point where the foot is completely down on the floor, the two sensor response curves intersect each other indicating equal pressure distribution. As the heel is lifted slowly while placing the toe ball down on the floor, the pressure of the toe ball increases up to a maximum and the pressure of the heel decreases to a minimum value. This behavior is repeated throughout the entire duration of walking, as shown by the sensor response plot in Figure 6c. The SSA was also applied for real-time running pressure variation monitoring. As shown by

DOI: 10.1021/acsami.9b11776
ACS Appl. Mater. Interfaces 2019, 11, 35201−35211

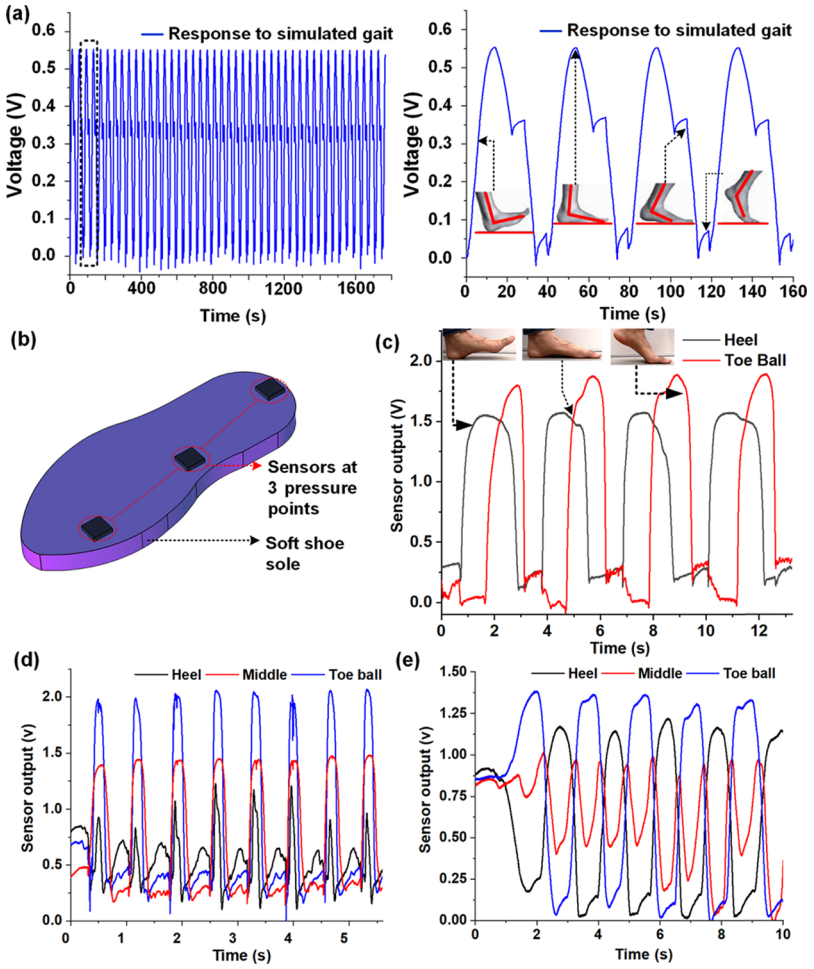

Figure 6. Application of the graphene-PDMS foam sensor for human gait monitoring: (a) response plot of the sensor to simulated gait; plot on the right shows the zoomed-in version of the sensor response over four gait cycles with schematics explaining heel positioning; (b) schematic representation of the soft shoe sole sensor assembly (SSA); (c) plot showing the sensor responses from the toe ball and heel regions while walking; (d) plot showing the sensor responses from the toe ball, foot arch, and heel regions while running; (e) plot showing sensor responses from the toe ball, foot arch, and heel regions while leaning forward and backward in a periodic fashion.

the plot in Figure 6d, the pressure response is very different from walking. In the case of running or jogging, most of the impact is absorbed by the toe ball followed by the middle arch, which is reflected clearly by the sensor response plot. Furthermore, the phase lag characteristics differ significantly from normal walking. To demonstrate the capability of the SSA in detecting pressure variation, the person wearing it leaned forward and backward in a periodic fashion leading to a periodic pressure distribution variation between the toe ball and the heel. As expected, the sensor response plot in Figure 6e clearly shows the phase lag between the toe ball and heel sensor pressure response. Interestingly, the pressure variation from the foot arch (middle sensor) is relatively less than those in the other two regions, which can be attributed to the fact that the maximum share of the weight of a human body is borne by the toe ball and heel, which leads to larger pressure concentration in those two regions in comparison to the foot arch region.

The fact that the maximum share of the weight of a human body is borne by the toe ball and heel (which leads to larger pressure concentration in those two regions in comparison to the foot arch region) was utilized to differentiate between a low arch (flat) foot and a medium arch foot using the SSA. Figure 7a compares a low arch/flat foot with a medium arch foot. Due to the difference in the anatomies of the two feet types, their pressure profiles are distinct and different. As seen in the figure, low arch-type foot typically has a foot arch sitting low to the ground, and hence, it has significantly more pressure concentration in the middle foot arch region in comparison to the medium arch foot. To demonstrate the capability of the SSA in distinguishing between the two different foot types, the setup was worn by a person with a flat foot, and the pressure response was recorded while the foot was placed down. The experiment was repeated on a person with a medium arch foot. The plots in Figure 7b show the SSA responses acquired from the persons with the two different foot types. As expected, the SSA response from the person with low arch/flat foot indicates a more even pressure distribution between the three pressure regions. Meanwhile, the SSA response acquired from the person with medium arch foot shows a more skewed pressure distribution with the toe ball and heel sharing the maximum share of the load in comparison to the middle arch region. The experiments demonstrate the capability of the SSA to distinguish between the different feet anatomies.

Furthermore, to demonstrate the applicability of the sensor in sensing finger and wrist joint movements, the sensor was secured on a wearable nitrile glove, which was then worn to demonstrate working on the sensor. Five cycles of finger and

DOI: 10.1021/acsami.9b11776
ACS Appl. Mater. Interfaces 2019, 11, 35201−35211

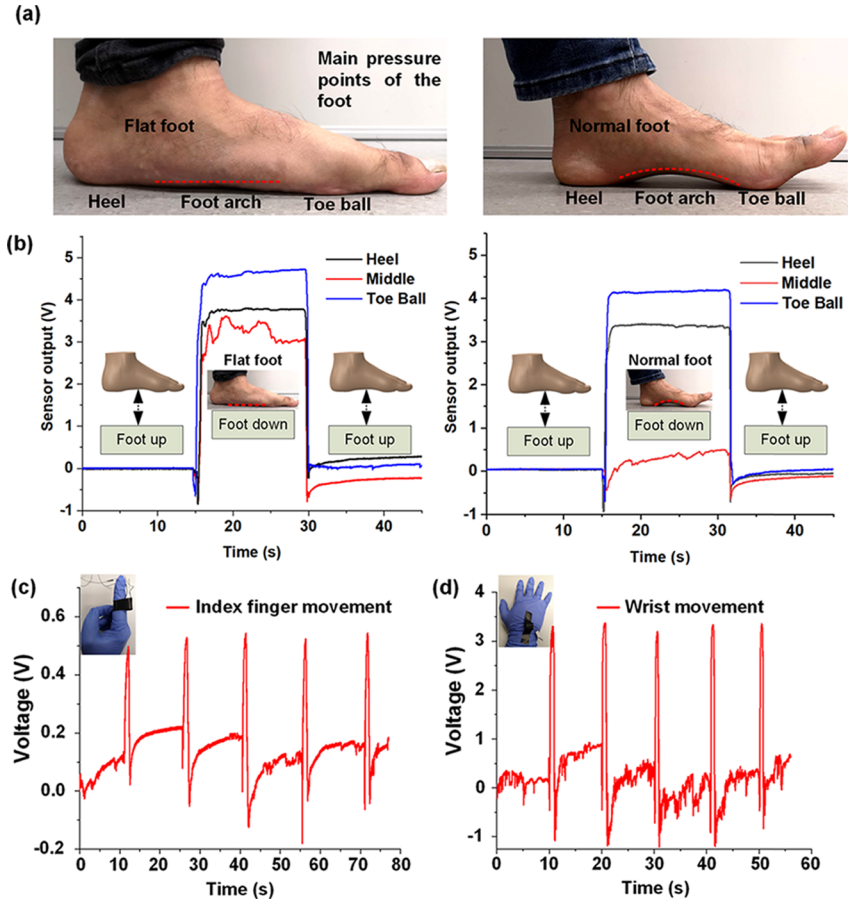

Figure 7. Application of the graphene-PDMS foam sensor for distinguishing between foot anatomies and human motion monitoring: (a) images comparing a low arch/flat foot with a medium arch biomechanically efficient foot; (b) plot comparing the SSA pressure responses acquired from the two different foot types. The pressure distribution in the case of the low arch foot is more even than that in the medium arch foot; (c) response of the sensor to index finger flick; (d) response of the sensor to wrist flick.

wrist flicking were carried out, and the output from the balanced Wheatstone bridge circuit to which the sensor was connected was recorded as shown in Figure 7c,d. The experiments conducted demonstrate the feasibility of using such sensors for developing wearable biomedical devices for health monitoring applications.

3. CONCLUSIONS

In conclusion, this work presented a facile method for developing a graphene-PDMS foam-based ultralightweight (having a density of 0.31 g cm^{-3}), squeezable, linear, and highly sensitive sensor. The sensor demonstrated in this work utilized a microporous PDMS substrate with graphene nanoflakes attached to its inner pore walls forming an MLG percolation network, which responds to pressure/strain by virtue of the conductive domain disconnection mechanism. To support the theory of conductive domain disconnection mechanism (which explains the strain-responsive resistance change property demonstrated by the sensor), SEM microscopic studies were conducted, which revealed the attachments of graphene nanoflakes on the inner pore walls of the PDMS foam substrate, thus backing up our hypothesis. The sensor was subjected to a series of static and dynamic strain stimuli response tests to evaluate its sensing performance and repeatability. The sensor responses were found to be linear, and the average gauge factor was determined to be 8.77 for compressive strains up to 9.5%. For compressive strains exceeding 10%, the gauge factor was found to vary between 2.87 and 8.77 (in the strain range of 10−50%). To demonstrate the feasibility of applying the sensor for various wearable devices and personalized health monitoring applications, both simulated and real-time gait responses and other human monitoring experiments were conducted. A soft shoe sole sensor assembly was fabricated and demonstrated to identify various gait characteristics, including walking, running, periodic leaning, and standing. The sensor assembly was also found to be capable of differentiating the foot types based on their middle arch architecture. The simple method for developing highly sensitive, lightweight, and squeezable piezoresistive sensors demonstrated in this work will inspire a future generation of inexpensive and highly efficient pressure and strain sensors suitable for human motion detection and personalized health monitoring applications.

4. EXPERIMENTAL METHODS

4.1. Preparation of PDMS Foam Base. Sundale extra-large sugar cubes were used as templates for fabricating PDMS foams. PDMS (Sylgard 184) acquired from Dow Corning was mixed in a ratio of 10:1 (base curing) to prepare the PDMS liquid and then degassed in a vacuum desiccator for 90 min to remove any unwanted trapped air bubbles. The sugar cubes were then dipped in the degassed liquid PDMS and placed in the vacuum desiccator for 90 min to let the liquid PDMS seep into the pores of the sugar cube template by capillary action. At the end of the desiccation procedure, the PDMS-loaded sugar cubes were cleaned to remove excess PDMS from their

DOI: 10.1021/acsami.9b11776
ACS Appl. Mater. Interfaces 2019, 11, 35201−35211

surfaces to avoid the formation of a skin layer, which could hinder the dissolution of sugar to release the PDMS foam. The cleaned PDMS-loaded sugar cubes were placed in an oven at 120 °C for 1 h to cure the PDMS. The cured PDMS-loaded sugar cubes were then placed in a sonicator bath at 40 °C for 1 h to dissolve the sugar template and release the PDMS foam structure.

4.2. Loading of the PDMS Foams with Graphene Nanoflakes. To fabricate piezoresistive graphene-PDMS foam sensors, the PDMS foams were loaded with graphene nanoflakes by immersing them in a sonicated homogeneous graphene suspension solution prepared by mixing 200 mg of 1.6 nm thick graphene nanoflakes (AO-1) acquired from Graphene Supermarket in 100 mL of *N*,*N*-dimethylformamide. Figure 1a shows the process steps involved in the loading procedure. In total, six dip coating cycles were conducted where each dip coating cycle comprised immersion of the PDMS foams in the graphene suspension followed by air-drying in an oven at 60 °C for 1 h.

4.3. Preparation of the Graphene-PDMS Foam Sensor. Epotek H20E conductive epoxy was used for making the electrical contacts for acquiring signal from the sensor. The parts A and B of the epoxy kit were mixed in a ratio of 1:1, smeared on two opposite faces of the foam, and subsequently cured at 120 °C for 20 min. Figure 1b shows the schematic representation of the graphene-PDMS foam sensor. Thin multistrand electrical wires were used for connecting the sensors to an appropriate Wheatstone bridge circuit.

4.4. Morphological Study. A Philips FEI XL30 environmental scanning electron microscope was employed to study the morphological properties of both the unloaded and graphene-loaded PDMS foams. Samples having dimensions of 2 cm × 2 cm × 2 cm were sputtered with gold and placed on an appropriate SEM stub. An acceleration voltage of 15 kV and a spot size of 3.0 were used while maintaining a working distance of 7 mm for carrying out the imaging studies.

4.5. Pressure/Strain Sensor Characterization Experiment. To characterize the performance of the graphene-PDMS foam sensor for pressure/strain sensing applications, Instron 5940 Universal Testing Systems with modified sample holders (appropriate for compressive tests) having a maximum force capacity of 2 kN was employed. To determine the compressive gauge factor of the sensor, a program was developed in the accompanying BlueHill software whereby the movable piston of the instrument was programed to move in steps of 50 μm to achieve a total compression of 0.95 mm in the foam sensor followed by stepwise relaxation (step size of 50 μm) all the way back to the original starting position. A compression step of 50 μm led to a compressive strain of 0.5% in the cubic sponge having an edge length 10 mm (after applying a 1% precompression). The copper pistons of the instrument doubled as the contact electrodes for acquiring electrical signals as shown in Figure 4a. The foam was connected to an appropriate Wheatstone bridge circuit, which converted the resistance change in the sponge to a voltage signal output. The signal output from the balanced Wheatstone bridge circuit was continuously acquired using a National Instruments data acquisition system (DAQ, NI USB-6009) and logged using National Instruments Signal express software as schematically shown in Figure 4a. The experiment was repeated thrice to observe consistency in the measurements.

To assess the strain sensing performance of the graphene-PDMS foam sensor for larger strain percentages, the sensor was subjected to five different maximum compressive cyclic strains (10, 20, 30, 40, and 50%) at a constant frequency of 5 Hz using a minishaker setup as schematically presented in Figure4c. An appropriate Wheatstone bridge circuit was designed to which the strain sensor was connected as an arm. The sensor was placed and secured between two glass plates, and a series of cyclic compressive stimuli were applied to the sensor employing a 120 mm long steel rod having a diameter of 2 mm connected to a Brüel & Kjær permanent magnet minishaker as shown in Figure 4c. The minishaker was driven at 5 Hz frequency using a Rigol function generator connected to a Brüel & Kjær (model number 2718) power amplifier, which generated a cyclic compressive strain in the graphene-PDMS sensor. The experiments were repeated for five different maximum strain percentages, namely, 10, 20, 30, 40, and 50%. The voltage output from the Wheatstone bridge circuit was acquired by employing the National Instruments data acquisition system (DAQ, NI USB-6009) and recorded using National Instruments Signal express software at a sampling rate of 1 kHz.

The reliability of the sensor was studied by subjecting it to a series of 36000 cyclic compressive loading and unloading at 5% compressive strain using the same experimental setup previously shown in Figure4c. The minishaker was driven at a constant frequency of 10 Hz, and the power amplifier driving the setup was set such that the compressive strain generated was approximately 5%. Like in the previous case, data was logged continuously by connecting the sensor to a Wheatstone bridge circuit to generate a voltage signal output and recording by employing the same data acquisition setup described previously.

4.6. Dynamic Sensing Performance Characterization Experiment. For evaluating the dynamic pressure/strain sensing performance of the graphene-PDMS foam sensor, the sensor was subjected to compressive strains at three different frequencies using the same minishaker setup described previously. The sensor was driven at 10, 35, and 70 Hz frequencies using a Rigol function generator connected to a Brüel & Kjær (model number 2718) power amplifier. The voltage output from the Wheatstone bridge circuit was acquired by employing the National Instruments data acquisition system (DAQ, NI USB-6009) and recorded using National Instruments Signal express software at a sampling rate of 1 kHz.

4.7. Sensor Applications in Gait Monitoring and Human Motion Detection. For the gait simulation experiment to demonstrate the gait monitoring capability of the graphene-PDMS foam sensor, the same setup described previously in the case of the pressure/strain sensor characterization experiment was employed. A program was developed in the Bluehill software whereby the piston moved with a constant speed of 20 mm/min to achieve a peak compressive force of 20 N for 10 s followed by a ramp down at the same speed to an intermediate compressive force of 3 N for 5 s before finally ramping all the way down to 0 N. The test was repeated for 45 cycles to observe the overall consistency in sensor response. For real-time gait and walking monitoring applications, three identical sensors were placed on a flat soft shoe sole and secured properly as schematically represented in Figure 6b. The sensors were connected to appropriate Wheatstone bridge circuits for continuous data logging. Experiments involving walking, running, and leaning in a periodic fashion were conducted on the shoe sole sensor assembly. The setup was also used for differentiating between a low arch/flat foot and a medium arch foot. For demonstrating the capability of the foam sensor for wearable applications, the electrically bonded sensors were secured on nitrile gloves as shown in the insets of Figure 7c,d. The gloves were worn, five cycles of index finger and wrist flicking were conducted, and the sensor responses were acquired. For all the experiments, data was logged continuously using the data acquisition setup described previously.

■ ASSOCIATED CONTENT

Supporting Information

The Supporting Information is available free of charge on the ACS Publications website at DOI: 10.1021/acsami.9b11776.

Squeezing the graphene-PDMS sensor with two fingers (MP4)

■ AUTHOR INFORMATION

Corresponding Author

*E-mail: a.g.p.kottapalli@rug.nl.

ORCID

Yutao Pei: 0000-0002-1817-2228

Ajay Giri Prakash Kottapalli: 0000-0002-3868-7069

DOI: 10.1021/acsami.9b11776
ACS Appl. Mater. Interfaces 2019, 11, 35201−35211

Author Contributions

D.S. conducted the graphene-PDMS foam sensor fabrication, sensor testing, and the associated data analysis and wrote the manuscript. A.G.P.K. conceptualized the idea, composed the experimental plan, and supervised the project. All the authors contributed to the discussion of the results and to the critical reading of the manuscript. A.G.P.K. and Y.P. supervised the research.

Funding

This research was supported by the University of Groningen's start-up grant awarded to A.G.P.K. The study was also supported by grants from the MIT Sea Grants program.

Notes

The authors declare no competing financial interest.

■ ACKNOWLEDGMENTS

The authors would like to thank Ms. Jessica Zotelli, who assisted the first author in preparing the sensors and conducted preliminary data analysis as a part of her master's thesis. We would also like to express our sincere gratitude to Prof. Dr. Beatriz Noheda Pinuaga from Zerinke Institute for Advanced Materials (ZIAM) and Dr. Mónica Isela Acuautla Meneses from Engineering and Technology Institute Groningen (ENTEG) for providing training and access to Instron 5940 UTS.

■ REFERENCES

(1) Wall, J. C.; Turnbull, G. I. Gait Asymmetries in Residual Hemiplegia. *Arch. Phys. Med. Rehabil.* **1986**, *67*, 550−553.

(2) Aktakka, E. E.; Peterson, R. L.; Najafi, K. A CMOS-Compatible Piezoelectric Vibration Energy Scavenger Based on the Integration of Bulk PZT Films on Silicon. In *Technical Digest - International Electron Devices Meeting, IEDM*; IEEE, 2010, 31−35.

(3) Wang, X. Y.; Lee, C. Y.; Peng, C. J.; Chen, P. Y.; Chang, P. Z. A Micrometer Scale and Low Temperature PZT Thick Film MEMS Process Utilizing an Aerosol Deposition Method. *Sens. Actuators, A* **2008**, *143*, 469−474.

(4) Chen, X.; Xu, S.; Yao, N.; Shi, Y. 1.6 V Nanogenerator for Mechanical Energy Harvesting Using PZT Nanofibers. *Nano Lett.* **2010**, *10*, 2133−2137.

(5) Wang, Z. L.; Song, J. Piezoelectric Nanogenerators Based on Zinc Oxide Nanowire Arrays. *Science* **2006**, *312*, 242−246.

(6) Qin, Y.; Wang, X.; Wang, Z. L. Microfibre-Nanowire Hybrid Structure for Energy Scavenging. *Nature* **2008**, *451*, 809−813.

(7) Wang, X.; Song, J.; Liu, J.; Wang, Z. L. Direct-Current Nanogenerator Driven by Ultrasonic Waves. *Science* **2007**, *316*, 102−105.

(8) Sengupta, D.; Kottapalli, A. G. P.; Chen, S. H.; Miao, J. M.; Kwok, C. Y.; Triantafyllou, M. S.; Warkiani, M. E.; Asadnia, M. Characterization of Single Polyvinylidene Fluoride (PVDF) Nanofiber for Flow Sensing Applications. *AIP Adv.* **2017**, *7*, 105205.

(9) Liu, Z. H.; Pan, C. T.; Lin, L. W.; Huang, J. C.; Ou, Z. Y. Direct-Write PVDF Nonwoven Fiber Fabric Energy Harvesters via the Hollow Cylindrical near-Field Electrospinning Process. *Smart Mater. Struct.* **2014**, *23*, 025003.

(10) Sencadas, V.; Moreira, M. V.; Lanceros-Méndez, S.; Pouzada, A. S.; Gregório Filho, R. α- to β Transformation on PVDF Films Obtained by Uniaxial Stretch. *Mater. Sci. Forum* **2006**, *514-516*, 872−876.

(11) Dargaville, T. R. T.; Celina, M. C.; Elliot, J.; Chaplya, P. M.; Elliott, J. M.; Jones, G. D.; Mowery, D. M.; Assink, R. a; Clough, R. L.; Martin, J. W. *Characterization, Performance and Optimization of PVDF as a Piezoelectric Film for Advanced Space Mirror Concepts. Optimization* 2005, SAND2005−6846, Sandia National Laboratories.

(12) Wang, Y. R.; Zheng, J. M.; Ren, G. Y.; Zhang, P. H.; Xu, C. A Flexible Piezoelectric Force Sensor Based on PVDF Fabrics. *Smart Mater. Struct.* **2011**, *20*, No. 045009.

(13) Cao, L.; Kim, T. S.; Mantell, S. C.; Polla, D. L. Simulation and Fabrication of Piezoresistive Membrane Type MEMS Strain Sensors. *Sens. Actuators, A* **2000**, *80*, 273−279.

(14) Da Silva, J. G.; De Carvalho, A. A.; Da Silva, D. D. A Strain Gauge Tactile Sensor for Finger-Mounted Applications. *IEEE Trans. Instrum. Meas.* **2002**, *51*, 18−22.

(15) Alamusi; Hu, N.; Fukunaga, H.; Atobe, S.; Liu, Y.; Li, J. Piezoresistive Strain Sensors Made from Carbon Nanotubes Based Polymer Nanocomposites. *Sensors* **2011**, *11*, 10691−10723.

(16) Pang, Y.; Tian, H.; Tao, L.; Li, Y.; Wang, X.; Deng, N.; Yang, Y.; Ren, T.-L. Flexible, Highly Sensitive, and Wearable Pressure and Strain Sensors with Graphene Porous Network Structure. *ACS Appl. Mater. Interfaces* **2016**, *8*, 26458−26462.

(17) Zhao, J.; He, C.; Yang, R.; Shi, Z.; Cheng, M.; Yang, W.; Xie, G.; Wang, D.; Shi, D.; Zhang, G. Ultra-Sensitive Strain Sensors Based on Piezoresistive Nanographene Films. *Appl. Phys. Lett.* **2012**, *101*, No. 063112.

(18) Amjadi, M.; Yoon, Y. J.; Park, I. Ultra-Stretchable and Skin-Mountable Strain Sensors Using Carbon Nanotubes-Ecoflex Nanocomposites. *Nanotechnology* **2015**, *26*, 375501.

(19) Amjadi, M.; Pichitpajongkit, A.; Lee, S.; Ryu, S.; Park, I. Highly Stretchable and Sensitive Strain Sensor Based on Silver Nanowire−Elastomer Nanocomposite. *ACS Nano* **2014**, 5154−5163.

(20) Thuau, D.; Ayela, C.; Poulin, P.; Dufour, I. Highly Piezoresistive Hybrid MEMS Sensors. *Sens. Actuators, A* **2014**, *209*, 161−168.

(21) Wisitsoraat, A.; Patthanasetakul, V.; Lomas, T.; Tuantranont, A. Low Cost Thin Film Based Piezoresistive MEMS Tactile Sensor. *Sens. Actuators, A* **2007**, *139*, 17−22.

(22) Qin, Y.; Peng, Q.; Ding, Y.; Lin, Z.; Wang, C.; Li, Y.; Xu, F.; Li, J.; Yuan, Y.; He, X.; Li, Y. Lightweight, Superelastic, and Mechanically Flexible Graphene/Polyimide Nanocomposite Foam for Strain Sensor Application. *ACS Nano* **2015**, *9*, 8933−8941.

(23) Yao, H.-B.; Ge, J.; Wang, C.-F.; Wang, X.; Hu, W.; Zheng, Z.-J.; Ni, Y.; Yu, S.-H. A Flexible and Highly Pressure-Sensitive Graphene − Polyurethane Sponge Based on Fractured Microstructure Design. *Adv. Mater.* **2013**, *25*, 6692−6698.

(24) Boland, C. S.; Khan, U.; Backes, C.; O'Neill, A.; McCauley, J.; Duane, S.; Shanker, R.; Liu, Y.; Jurewicz, I.; Dalton, A. B.; et al. Sensitive, High-Strain, High-Rate Bodily Motion Sensors Based on Graphene-Rubber Composites. *ACS Nano* **2014**, *8*, 8819−8830.

(25) Li, Q.; Liu, H.; Zhang, S.; Zhang, D.; Liu, X.; He, Y.; Mi, L.; Zhang, J.; Liu, C.; Shen, C.; et al. Superhydrophobic Electrically Conductive Paper for Ultrasensitive Strain Sensor with Excellent Anticorrosion and Self-Cleaning Property. *ACS Appl. Mater. Interfaces* **2019**, *11*, 21904−21914.

(26) Yamada, T.; Hayamizu, Y.; Yamamoto, Y.; Yomogida, Y.; Izadi-Najafabadi, A.; Futaba, D. N.; Hata, K. A Stretchable Carbon Nanotube Strain Sensor for Human-Motion Detection. *Nat. Nanotechnol.* **2011**, *6*, 296.

(27) Kong, J.-H.; Jang, N.-S.; Kim, S.-H.; Kim, J.-M. Simple and Rapid Micropatterning of Conductive Carbon Composites and Its Application to Elastic Strain Sensors. *Carbon* **2014**, *77*, 199−207.

(28) Sengupta, D.; Kottapalli, A. G. P.; Chen, S. H.; Michael, A.; Kwok, C. Y.; Miao, J.; Triantafyllou, M. S. Flexible Graphitized Polyacrylonitrile Nanofiber Bundles for Strain Sensors. In *NEMS 2018 - 13th Annual IEEE International Conference on Nano/Micro Engineered and Molecular Systems*; IEEE, 2018.

(29) Liu, H.; Dong, M.; Huang, W.; Gao, J.; Dai, K.; Guo, J.; Zheng, G.; Liu, C.; Shen, C.; Guo, Z. Lightweight Conductive Graphene/Thermoplastic Polyurethane Foams with Ultrahigh Compressibility for Piezoresistive Sensing. *J. Mater. Chem. C* **2017**, *5*, 73−83.

(30) Zhang, S.; Liu, H.; Yang, S.; Shi, X.; Zhang, D.; Shan, C.; Mi, L.; Liu, C.; Shen, C.; Guo, Z. Ultrasensitive and Highly Compressible Piezoresistive Sensor Based on Polyurethane Sponge Coated with a

DOI: 10.1021/acsami.9b11776
ACS Appl. Mater. Interfaces 2019, 11, 35201−35211

Cracked Cellulose Nanofibril/Silver Nanowire Layer. *ACS Appl. Mater. Interfaces* **2019**, *11*, 10922−10932.
(31) Huang, T.; He, P.; Wang, R.; Yang, S.; Sun, J.; Xie, X.; Ding, G. Porous Fibers Composed of Polymer Nanoball Decorated Graphene for Wearable and Highly Sensitive Strain Sensors. *Adv. Funct. Mater.* **2019**, 1903732.
(32) Liu, Q.; Chen, J.; Li, Y.; Shi, G. High-Performance Strain Sensors with Fish-Scale-Like Graphene-Sensing Layers for Full-Range Detection of Human Motions. *ACS Nano* **2016**, *10*, 7901−7906.
(33) Rinaldi, A.; Tamburrano, A.; Fortunato, M.; Sarto, M. A Flexible and Highly Sensitive Pressure Sensor Based on a PDMS Foam Coated with Graphene Nanoplatelets. *Sensors* **2016**, *16*, 2148.
(34) Cheng, Y.; Wang, R.; Sun, J.; Gao, L. A Stretchable and Highly Sensitive Graphene-Based Fiber for Sensing Tensile Strain, Bending, and Torsion. *Adv. Mater.* **2015**, 7365.
(35) Liu, H.; Li, Q.; Zhang, S.; Yin, R.; Liu, X.; He, Y.; Dai, K.; Shan, C.; Guo, J.; Liu, C.; et al. Electrically Conductive Polymer Composites for Smart Flexible Strain Sensors: A Critical Review. *J. Mater. Chem. C* **2018**, *6*, 12121−12141.
(36) Tran, D. N. H.; Kabiri, S.; Sim, T. R.; Losic, D. Selective Adsorption of Oil−Water Mixtures Using Polydimethylsiloxane (PDMS)−Graphene Sponges. *Environ Sci: Water Res Technol* **2015**, *1*, 298−305.
(37) Nguyen, D. D.; Tai, N. H.; Lee, S. B.; Kuo, W. S. Superhydrophobic and Superoleophilic Properties of Graphene-Based Sponges Fabricated Using a Facile Dip Coating Method. *Energy Environ. Sci.* **2012**, *5*, 7908−7912.
(38) Liu, Y.; Ma, J.; Wu, T.; Wang, X.; Huang, G.; Liu, Y.; Qiu, H.; Li, Y.; Wang, W.; Gao, J. Cost-Effective Reduced Graphene Oxide-Coated Polyurethane Sponge as a Highly Efficient and Reusable Oil-Absorbent. *ACS Appl. Mater. Interfaces* **2013**, *5*, 10018−10026.
(39) Xiao, X.; Yuan, L.; Zhong, J.; Ding, T.; Liu, Y.; Cai, Z.; Rong, Y.; Han, H.; Zhou, J.; Wang, Z. L. High-Strain Sensors Based on ZnO Nanowire / Polystyrene Hybridized Flexible Films. *Adv. Mater.* **2011**, *23*, 5440−5444.
(40) Hempel, M.; Nezich, D.; Kong, J.; Hofmann, M. A Novel Class of Strain Gauges Based on Layered Percolative Films of 2D Materials. *Nano Lett.* **2012**, *12*, 5714−5718.
(41) Park, J. J.; Hyun, W. J.; Mun, S. C.; Park, Y. T.; Park, O. O. Highly Stretchable and Wearable Graphene Strain Sensors with Controllable Sensitivity for Human Motion Monitoring. *ACS Appl. Mater. Interfaces* **2015**, *7*, 6317−6324.
(42) Amjadi, M.; Kyung, K.-U.; Park, I.; Sitti, M. Stretchable , Skin-Mountable , and Wearable Strain Sensors and Their Potential Applications : A Review. *Adv. Funct. Mater.* **2016**, *26*, 1678−1698.
(43) Oskouyi, A. B.; Sundararaj, U.; Mertiny, P. A Numerical Model to Study the Effect of Temperature on Electrical Conductivity of Polymer-CNT Nanocomposites. In *ASME 2013 International Mechanical Engineering Congress and Exposition*; American Society of Mechanical Engineers Digital Collection, 2014.
(44) Hicks, J.; Behnam, A.; Ural, A. A Computational Study of Tunneling-Percolation Electrical Transport in Graphene-Based Nanocomposites. *Appl. Phys. Lett.* **2009**, *95*, 213103.
(45) Charara, M.; Luo, W.; Saha, M. C.; Liu, Y. Investigation of Lightweight and Flexible Carbon Nanofiber/Poly Dimethylsiloxane Nanocomposite Sponge for Piezoresistive Sensor Application. *Adv. Eng. Mater.* **2019**, *21*, 1801068.
(46) Muth, J. T.; Vogt, D. M.; Truby, R. L.; Mengüç, Y.; Kolesky, D. B.; Wood, R. J.; Lewis, J. A. Embedded 3D Printing of Strain Sensors within Highly Stretchable Elastomers. *Adv. Mater.* **2014**, *26*, 6307−6312.
(47) Cai, J.; Chawla, S.; Naraghi, M. Piezoresistive Effect of Individual Electrospun Carbon Nanofibers for Strain Sensing. *Carbon* **2014**, *77*, 738−746.
(48) Kamat, A. M.; Pei, Y.; Kottapalli, A. G. P. Bioinspired Cilia Sensors with Graphene Sensing Elements Fabricated Using 3D Printing and Casting. *Nanomaterials* **2019**, *9*, 954.
(49) Chi, K. J.; Schmitt, D. Mechanical Energy and Effective Foot Mass during Impact Loading of Walking and Running. *J. Biomech.* **2005**, *38*, 1387−1395.
(50) Murray, M. P.; Kory, R. C.; Clarkson, B. H. Walking Patterns in Healthy Old Men. *J. Gerontol.* **1969**, *24*, 169−178.

DOI: 10.1021/acsami.9b11776
ACS Appl. Mater. Interfaces 2019, 11, 35201−35211